applied sciences

MDPI

Article

Performance Prediction of High-Speed Hydrogen Gas-Lubricated Herringbone Grooved Journal Bearing

Mingchen Qiang, Qi Zhao, Shaohang Yan, Xue Liu, Yu Hou and Tianwei Lai *

School of Energy and Power Engineering, Xi'an Jiaotong University, Xi'an 710049, China; qmc990223@stu.xjtu.edu.cn (M.Q.); wheredream2012@stu.xjtu.edu.cn (Q.Z.); ysh1040014659@stu.xjtu.edu.cn (S.Y.); liuxuewith@stu.xjtu.edu.cn (X.L.); yuhou@mail.xjtu.edu.cn (Y.H.)
* Correspondence: laitianwei@mail.xjtu.edu.cn; Tel.: +86-152-0295-2214

Abstract: The liquefaction of hydrogen is considered to be a crucial process in the large-scale utilization of hydrogen energy. In hydrogen liquefaction, hydrogen turbo-expander is a key refrigerating machine for high liquefaction efficiency. Performance of the turbo-expander is directly affected by the hydrogen gas bearings. To obtain a deep understanding of the performance characteristics of hydrogen gas bearings, the static and dynamic characteristics of herringbone grooved journal bearings under hydrogen and other lubricating gases were numerically calculated and compared. The bearing load capacity and critical mass of hydrogen gas bearings were slightly lower than those of helium-, air- and nitrogen-lubricated bearings. To improve the performance of the hydrogen gas bearings used in high-speed turbo-machinery, the influence of working conditions was analyzed. It is found that the load capacity of hydrogen gas bearings can be improved by increasing the ambient pressure, reducing the gas film clearance, and raising the bearing eccentricity ratio. Meanwhile, the critical mass increases, and the bearing dynamic stability is enhanced.

Keywords: hydrogen energy; herringbone grooved journal bearing; hydrogen lubrication; bearing performance

Citation: Qiang, M.; Zhao, Q.; Yan, S.; Liu, X.; Hou, Y.; Lai, T. Performance Prediction of High-Speed Hydrogen Gas-Lubricated Herringbone Grooved Journal Bearing. *Appl. Sci.* **2022**, *12*, 6432. https://doi.org/10.3390/app12136432

Academic Editors: Marek Krawczuk and Magdalena Palacz

Received: 11 May 2022
Accepted: 20 June 2022
Published: 24 June 2022

1. Introduction

Hydrogen is regarded as a source of green energy, because it is non-toxic, pollution-free, and makes zero contribution to the greenhouse effect. At present, the utilization of hydrogen energy mainly consists of the following aspects: hydrogen-powered vehicles, hydrogen power generation, molten carbonate fuels, and solid oxide batteries [1–4]. Related technologies are drawing increasing attention [1].

For the storage and large-scale utilization of hydrogen energy, liquid-state hydrogen is indispensable, compared to gaseous and solid storage states, due to its high storage efficiency and high energy density [5–7]. For hydrogen liquefaction, the Brayton cycle and the Claude cycle are often used. The optimized design of the liquefaction cycle consists of pre-cooling, throttling, and circulation processes [8,9]. The hydrogen turbo-expander is the main piece of refrigeration equipment employed in the process of hydrogen liquefaction. The cycle efficiency and yield of the hydrogen liquefaction process are greatly affected by the performance of the hydrogen turbo-expander [10].

As a key component, the performance of high-speed gas bearings is significant factor influencing the reliability of turbo-expander [11]. Depending on their working mechanism, gas bearings can be categorized into aerostatic bearings and aerodynamic bearings. With aerostatic bearings, external air is used to provide the required bearing load capacity. For aerodynamic bearings, there is no external gas supply. Their load capacity is generated by the viscosity of the gas and the high-speed shear effect in the wedge-shaped clearance. Generally speaking, aerodynamic bearings have good adaptability. Compared with other aerodynamic journal bearings with rigid surfaces, herringbone grooved journal bearings

have high stability and adaptability due to the pumping effect of the grooves on gas [12]. Currently, herringbone grooved journal bearings have important applications in lightweight rotating machinery and high-precision equipment, and are widely used in gyroscopes, automotive turbochargers, turbo-compressors for refrigeration, etc. [13].

With respect to aerodynamic bearings, their performance with respect to aspects such as static load and dynamic stability are the most important research topics [14,15]. Li et al. found that friction torque, stiffness and punching performance were deeply affected by the parameters of herringbone grooved gas bearings. The bearing load capacity can be improved by increasing the groove angle, decreasing the width-to-ridge ratio, or increasing the groove circumferential ratio [16]. Li et al. explored the influence of geometric parameters on the performance parameters of aerodynamic bearings based on the CFD model. A new groove shape was proposed that was able to effectively improve the static and dynamic performance of the bearing [17]. Li et al. analyzed the influence of ambient pressure on the dynamic characteristics of gas foil bearings. It was found that the direct stiffness K_{xx} and K_{yy} and the direct damping D_{xx} and D_{yy} of the gas film increased with increasing ambient pressure [18]. Mark et al. reviewed the challenges presented by gas bearings operating at low temperatures. On the basis of experiments and analysis, several solutions were proposed to overcome these difficulties [19]. In recent years, more practical models and applications have been widely studied, including the real gas lubrication model, the rarefaction or turbulence model, and other physical models [13].

At present, most of the research on turbo-expanders is carried out with air as the working medium [20]. Conversely, there have been few studies on hydrogen turbo-expanders [21]. In the design process of cryogenic turbo-expanders, it is necessary to consider the influence of different lubricating media on the performance of gas-lubricated journal bearings. Guo et al. performed numerical calculations for bearings with different gaseous lubricants. It was found that the viscosity of gaseous lubricants had a significant impact on the bearing load capacity [22]. Yan et al. analyzed the differences in bearing performance using different gases, such as hydrogen, helium, and air. A more adaptable model was proposed, which was suitable for various lubricating media [23].

There are still no design criteria for hydrogen-lubricated aerodynamic bearings due to the low viscosity of hydrogen. The performance of hydrogen gas bearings is still not able to fully meet the high-speed requirements, which may cause major failures in hydrogen turbo-expanders. With the aim of improving bearing performance, the static and dynamic characteristics of hydrogen-lubricated herringbone grooved journal bearings are numerically studied. The bearing performances using hydrogen and other lubricating gases are compared. The effects of ambient pressure, gas film clearance and eccentricity ratio on bearing performance are evaluated.

2. Structure and Model

2.1. Herringbone Grooved Journal Bearing

The structural diagram of the bearing is shown in Figure 1. The structural parameters of the bearing are listed in Table 1. The key parameters of the structure are groove angle α, number of grooves N, groove depth h_g, film clearance c_0, eccentricity e, groove circumferential ratio L_0/L, and groove axial ratio $b_g/(b_g + b_r)$.

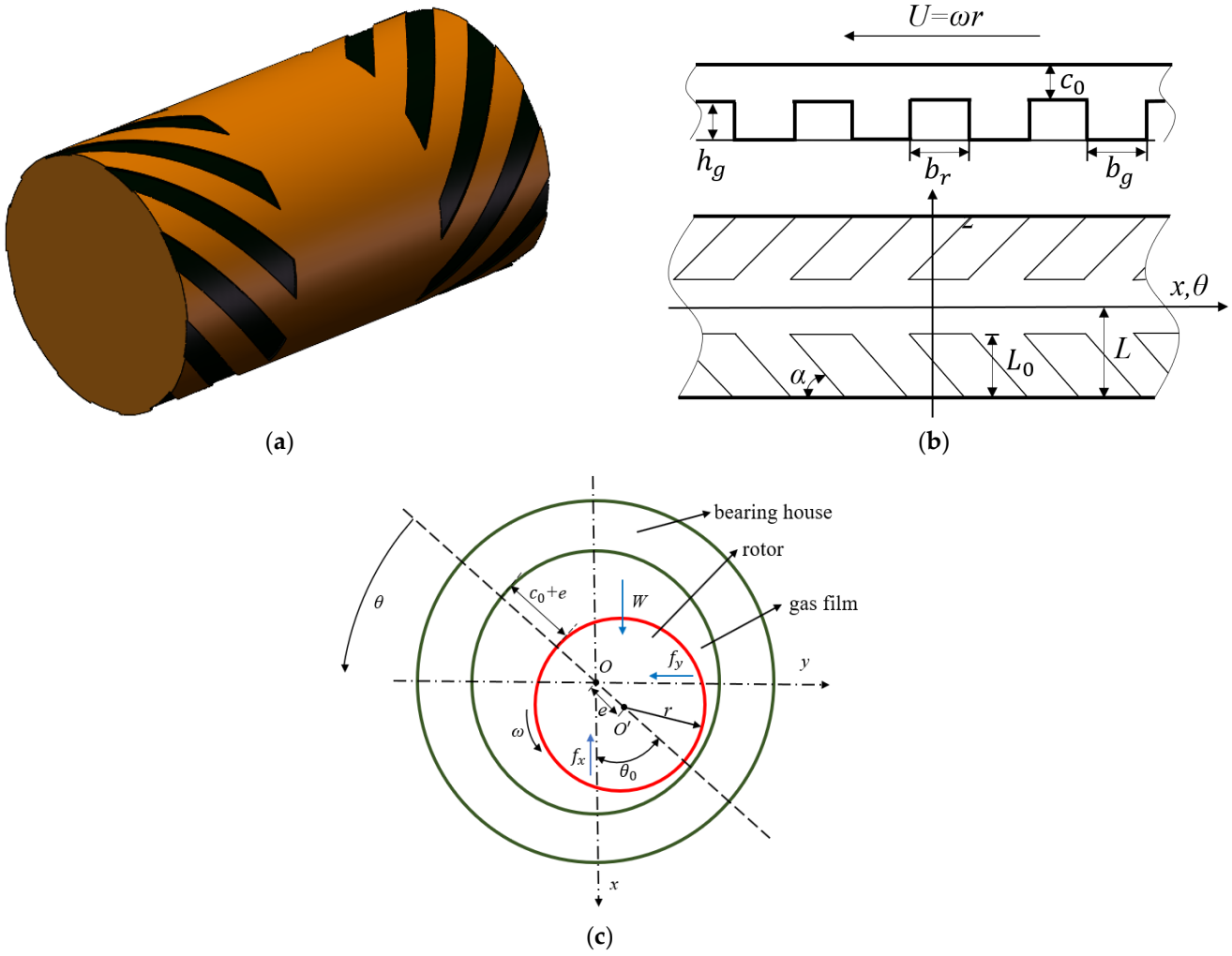

Figure 1. Schematic diagram of herringbone grooved journal bearing. (**a**) Three-dimensional structure; (**b**) expanded view; (**c**) cylindrical coordinate system.

Table 1. Structural parameters of herringbone grooved journal bearing.

Structural Parameters	Value	Unit
bearing length	40	mm
bearing radius	20	mm
film clearance	20	μm
groove depth	20	μm
groove angle	60	°
number of grooves	4	/
groove circumferential ratio	0.5	/
groove axial ratio	0.5	/
eccentricity ratio	0.5	/

2.2. Mathematical Model

To determine the pressure distribution in the gas film, the Reynolds equation is the basic governing equation, which is expressed as follows [24]:

$$\frac{\partial}{\partial x}\left(ph^3\frac{\partial p}{\partial x}\right)+\frac{\partial}{\partial z}\left(ph^3\frac{\partial p}{\partial z}\right)=6\mu U_0\frac{\partial}{\partial x}(ph)+12\mu\frac{\partial(\mathrm{ph})}{\partial t} \quad (1)$$

To simplify the calculation, it is assumed that the gas is isothermal ideal gas, and the gas rarefaction effect is ignored. The Reynolds number is calculated as follows [25]:

$$\mathrm{Re} = \frac{\rho r \omega c_0}{\mu} \tag{2}$$

where ρ represents density, r represents radius, ω represents rotational speed, c_0 represents gas film clearance, and μ represents dynamic viscosity. When the ambient pressure is 1.5 MPa and the rotational speed is 80,000 rpm, the Reynolds number of the gas film is only 152, and this flow pattern can be regarded as laminar flow. According to the coordinate system shown in Figure 1c, Equation (1) can be expressed as:

$$\frac{1}{r^2}\frac{\partial}{\partial\theta}\left(ph^3\frac{\partial p}{\partial\theta}\right) + \frac{\partial}{\partial z}\left(ph^3\frac{\partial p}{\partial z}\right) = 6\mu\omega\frac{\partial}{\partial\theta}(ph) + 12\mu\frac{\partial(\mathrm{ph})}{\partial t} \tag{3}$$

The following dimensionless quantities are introduced:

$$\begin{array}{c} P = p/p_a;\ x = r\theta; H = h/c_0;\ H_1 = h_g/c_0; \\ Z = z/r;\ T = \nu t;\ \gamma = \frac{\nu}{\omega}; \Lambda = \left(6\mu\omega r^2\right)/\left(p_a c_0^2\right) \end{array} \tag{4}$$

where c_0 represents bearing clearance, ω represents rotor speed, ν represents whirl frequency, μ represents gas dynamic viscosity, p_a represents ambient pressure, and Λ represents the bearing number. The dimensionless Reynolds equation is obtained as follows:

$$\frac{\partial}{\partial\theta}\left(PH^3\frac{\partial P}{\partial\theta}\right) + \frac{\partial}{\partial Z}\left(PH^3\frac{\partial P}{\partial Z}\right) = \Lambda\frac{\partial(PH)}{\partial\theta} + 2\Lambda\gamma\frac{\partial(PH)}{\partial \mathrm{T}} \tag{5}$$

To solve the above equation, the linear perturbation method is used. This method was proposed by Lund et al. and has been widely used and demonstrated to be very effective [26,27]. Therefore, the linear perturbation method is used to analyze the characteristics of the journal bearings.

Since the trajectory of the axis approximates an ellipse shape, a simple harmonic model is adopted. Dimensionless disturbances include the following:

$$\text{Displacement disturbance:} \quad \begin{cases} \Delta X = \frac{\Delta x}{c_0} = |\Delta X| \cdot e^{it} \\ \Delta Y = \frac{\Delta y}{c_0} = |\Delta Y| \cdot e^{it} \end{cases} \tag{6}$$

$$\text{Velocity disturbance:} \quad \begin{cases} \Delta \dot{X} = \frac{\partial \Delta X}{\partial T} = i \cdot \Delta X \\ \Delta \dot{Y} = \frac{\partial \Delta Y}{\partial T} = i \cdot \Delta Y \end{cases} \tag{7}$$

$$\text{Acceleration disturbance:} \quad \begin{cases} \Delta \ddot{X} = \frac{\partial \Delta \dot{X}}{\partial T} = -\Delta X \\ \Delta \ddot{Y} = \frac{\partial \Delta \dot{Y}}{\partial T} = -\Delta Y \end{cases} \tag{8}$$

Then, the dimensionless pressure and gas film clearance can be expressed as:

$$\begin{cases} P = P_0 + P_X \cdot \Delta X + P_X \cdot \Delta \dot{X} + P_Y \cdot \Delta Y + P_Y \cdot \Delta \dot{Y} \\ H = H_0 + H_X \cdot \Delta X + H_X \cdot \Delta \dot{X} + H_Y \cdot \Delta Y + H_Y \cdot \Delta \dot{Y} \end{cases} \tag{9}$$

On the basis of the distribution of static pressure p_0 and static clearance H_0, the static performance parameters of the bearing can be obtained through integration as follows:

$$\text{Dimensionless gas film force:} \begin{bmatrix} F_X \\ F_Y \end{bmatrix} = \frac{1}{p_a r^2}\begin{bmatrix} f_x \\ f_y \end{bmatrix} = \int_{-l/d}^{+l/d}\int_0^{2\pi}\begin{bmatrix} -P_0\cos\theta \\ -P_0\sin\theta \end{bmatrix} \mathrm{d}\theta \mathrm{d}Z \tag{10}$$

$$\text{Bearing load capacity:} \quad W = p_a r^2\sqrt{F_X^2 + F_Y^2} \tag{11}$$

$$\text{Bearing attitude angle:} \quad \theta_0^{k+1} = \tan^{-1}\left[\frac{F_X \sin\left(\theta_0^k\right) - F_Y \cos\left(\theta_0^k\right)}{F_X \cos\left(\theta_0^k\right) + F_Y \sin\left(\theta_0^k\right)}\right] \tag{12}$$

$$\text{Friction torque:} \quad f_t = p_a r^2 \int_{-l/d}^{+l/d} \int_0^{2\pi} \left[\frac{H_0}{2}\frac{\partial P_0}{\partial \theta} + \frac{\Lambda}{6H_0}\right] \mathrm{d}\theta \mathrm{d}Z \tag{13}$$

When the rotor has a low displacement disturbance $(\Delta x,\ \Delta y)$ and a velocity disturbance $\left(\Delta \dot{x},\ \Delta \dot{y}\right)$ close to the balance position, the gas film force can be expressed as:

$$F = F_0 + \left(\frac{\partial F}{\partial X}\right)_0 \Delta X + \left(\frac{\partial F}{\partial Y}\right)_0 \Delta Y + \left(\frac{\partial F}{\partial \dot{X}}\right)_0 \Delta \dot{X} + \left(\frac{\partial F}{\partial \dot{Y}}\right)_0 \Delta \dot{Y} + O\left(X^2 + Y^2 + \dot{X}^2 + Y^2\right) \tag{14}$$

where the subscript "0" represents the static balance position. Then, the dimensionless stiffness coefficient and dimensionless damping coefficient of the bearing can be expressed as:

$$\text{Dimensionless stiffness coefficient:} \begin{bmatrix} K_{xx} & K_{yx} \\ K_{xy} & K_{yy} \end{bmatrix} = \frac{k}{p_a r^2} \begin{bmatrix} k_{xx} & k_{yx} \\ k_{xy} & k_{yy} \end{bmatrix} = \left(\begin{bmatrix} \frac{\partial F}{\partial X} \\ \frac{\partial F}{\partial Y} \end{bmatrix} \right)_0 \tag{15}$$

$$\text{Dimensionless damping coefficient:} \begin{bmatrix} D_{xx} & D_{yx} \\ D_{xy} & D_{yy} \end{bmatrix} = \frac{c_0}{p_a r^2} \begin{bmatrix} d_{xx} & d_{yx} \\ d_{xy} & d_{yy} \end{bmatrix} = \left(\begin{bmatrix} \frac{\partial F}{\partial \dot{X}} \\ \frac{\partial F}{\partial \dot{Y}} \end{bmatrix} \right)_0 \tag{16}$$

The rigid symmetrical rotor model is used to analyze the stability, and the rotor mass is assumed to be 2 M. Then, the motion equation of a small disturbance close to the balance position of the rotor can be obtained as follows:

$$\begin{cases} M\Delta \ddot{x} + k_{xx}\Delta x + k_{xy}\Delta y + d_{xx}\Delta \dot{x} + d_{xy}\Delta \dot{y} = 0 \\ M\Delta \ddot{y} + k_{yx}\Delta x + k_{yy}\Delta y + d_{yx}\Delta \dot{x} + d_{yy}\Delta \dot{y} = 0 \end{cases} \tag{17}$$

The solution of $\Delta x,\ \Delta y$ is assumed to take the following form:

$$\begin{cases} \Delta x = \Delta x_0 e^{st} \\ \Delta y = \Delta y_0 e^{st} \end{cases} \tag{18}$$

where $s = \lambda + i\nu$, λ is the system damping coefficient, and ν is whirl frequency. In the critical state, the system damping is zero, that is, $\lambda = 0$. Under this condition, Equation (18) can be written as [28]:

$$\begin{bmatrix} Z_{xx} - \nu^2 M & Z_{xy} \\ Z_{yx} & Z_{yy} - \nu^2 M \end{bmatrix} \begin{bmatrix} \Delta x_0 \\ \Delta y_0 \end{bmatrix} = 0 \tag{19}$$

where $Z_{jk} = K_{jk} + i\nu D_{jk}$ is the compound stiffness. According to the Hurwitz stability criterion, the necessary and sufficient condition for the solution of Equation (19) is that its coefficient determinant is zero, that is:

$$\begin{vmatrix} Z_{xx} - \nu^2 M & Z_{xy} \\ Z_{yx} & Z_{yy} - \nu^2 M \end{vmatrix} = 0 \tag{20}$$

By solving Equation (20), the critical whirl ratio and the critical mass can be obtained:

$$\text{Critical whirl ratio:} \quad \gamma_{cr} = \frac{\nu}{\omega} = \sqrt{\frac{(K_{xx} - K_0)(K_{yy} - K_0) - K_{xy}K_{yx}}{D_{xx}D_{yy} - D_{xy}D_{yx}}} \tag{21}$$

$$\text{Critical mass:} \quad m_{cr} = \frac{p_a r^2 K_0}{c_0 \omega^2 \gamma_{cr}^2} \tag{22}$$

where K_0 represents the dimensionless critical stiffness coefficient:

$$K_0 = \frac{K_{xx}D_{yy} + K_{yy}D_{xx} - K_{xy}D_{yx} - K_{yx}D_{xy}}{D_{xx} + D_{yy}} \tag{23}$$

The calculation flow chart for this method is shown in Figure 2. First, the calculation parameters are input. The Reynolds equation is solved using the linear perturbation method, and the static gas film pressure and thickness distribution are obtained. Then, the convergence for the gas film pressure is checked. After the pressure converges, the load capacity, deflection angle, friction moment and dynamic gas film force are computed. Next, the critical whirl ratio is calculated, and its convergence is checked. Afterwards, the critical mass is computed. Finally, the calculation results are output.

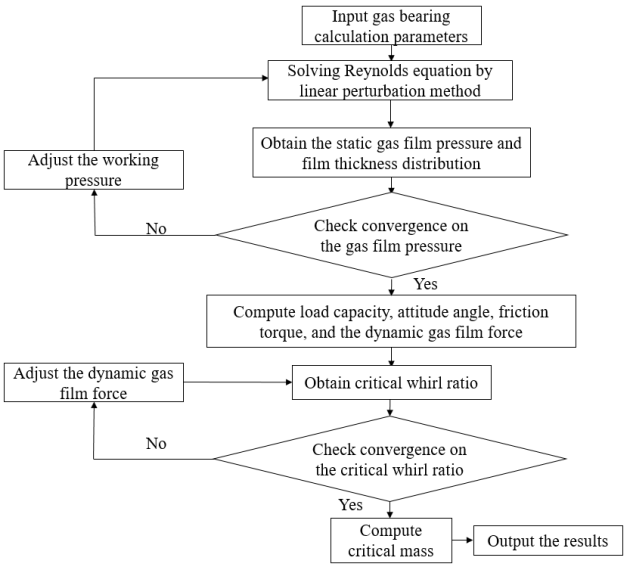

Figure 2. Flow chart of the calculation procedure.

2.3. Model Validation

To verify the model, the results obtained using the model are compared with those found in the literature [29]. The dimensionless load capacities of bearings with different eccentricity ratios under different numbers of bearings are shown in Figure 3. The calculation results presented in this paper are in good agreement with the data presented in the literature. The maximum relative error is less than 10%.

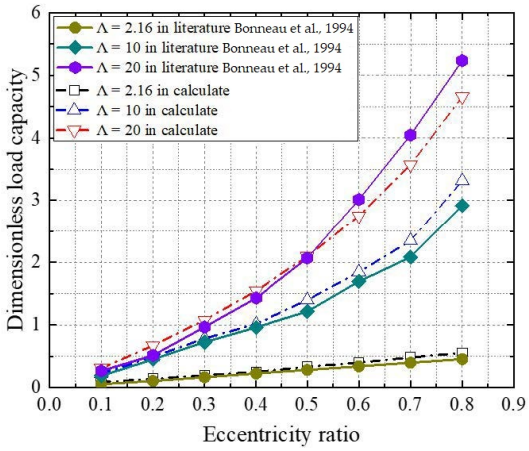

Figure 3. Model validation for dimensionless load capacity (length width ratio L/D = 1; groove angle α = 30°; number of grooves N = 4; film clearance c_0 = groove depth h_g = 10 μm) [29].

2.4. Pressure Field of Hydrogen-Lubricated Herringbone Grooved Journal Bearings

The dimensionless pressure field of a hydrogen gas bearing (ambient pressure of 0.5 MPa and ambient temperature of 300 K) is shown in Figure 4. The high-pressure zone is in the area where θ is around 3.2 (radian system). The maximum dimensionless pressure is about 1.16.

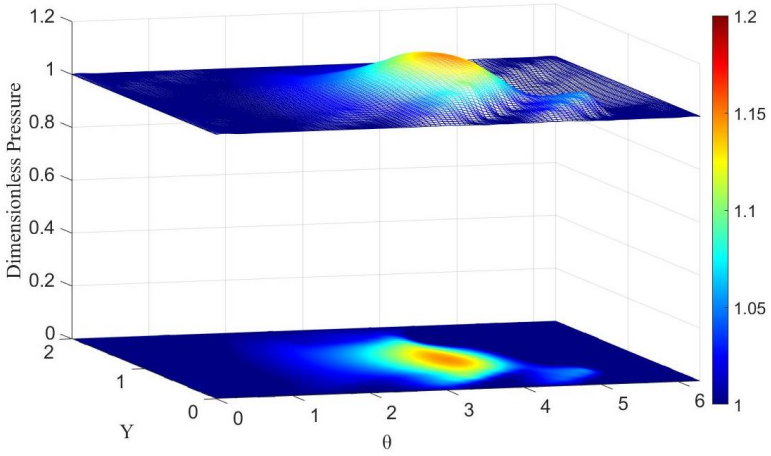

Figure 4. Dimensionless pressure field of hydrogen gas bearing (0.5 MPa, 300 K).

3. Comparison of Gaseous Lubricant

3.1. Physical Property Difference

The commonly used lubricating gases have similar physical properties, which can be analyzed based on the same model. In addition, the physical properties of different gaseous lubricants should be considered in application. Compared to commonly used gaseous lubricants such as air, nitrogen and helium, hydrogen lubricant has a lower density and viscosity, as shown in Figure 5. Thus, when designing hydrogen gas bearings, the lower density and viscosity need to be taken into consideration.

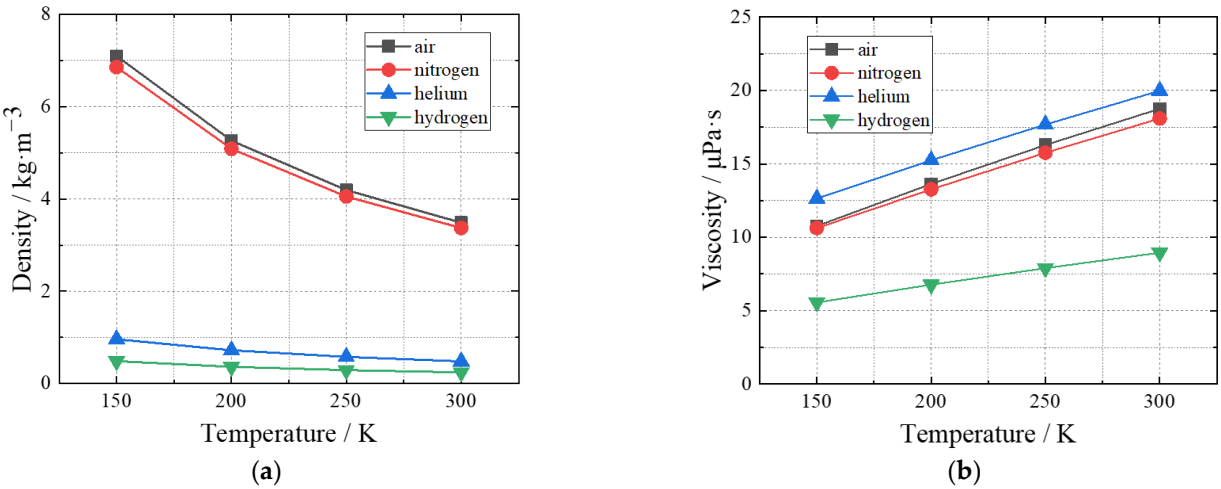

Figure 5. (**a**) Density and (**b**) viscosity of air, nitrogen, helium, and hydrogen with temperature (0.3 MPa).

3.2. Performance of Different Gas-Lubricated Bearings

To compare bearing performances, several different commonly used gases—air, nitrogen, helium and hydrogen—are selected. Bearing load capacity, friction torque and critical mass are used to quantify the performance of the hydrogen gas bearings. Load capacity is the physical quantity that reflects the basic performance of the bearing. Friction torque can be used to characterize the friction loss of the bearing. Critical mass is a dynamic performance parameter that represents the maximum rotor mass that the bearing is able to dynamically support, and reflects the dynamic stability of the bearing.

Bearing load capacities and attitude angles with rotational speed using different gases are shown in Figure 6. The bearing load capacity exhibits a linear growth trend with rotational speed. The bearing load capacity decreases in the order of helium, air, nitrogen and hydrogen. Moreover, the bearing capacities of air-, nitrogen- and helium-lubricated

bearings become closer, and are far higher than that of the hydrogen gas-lubricated bearing. Throughout the whole speed range, the attitude angle of the hydrogen gas bearing is the largest.

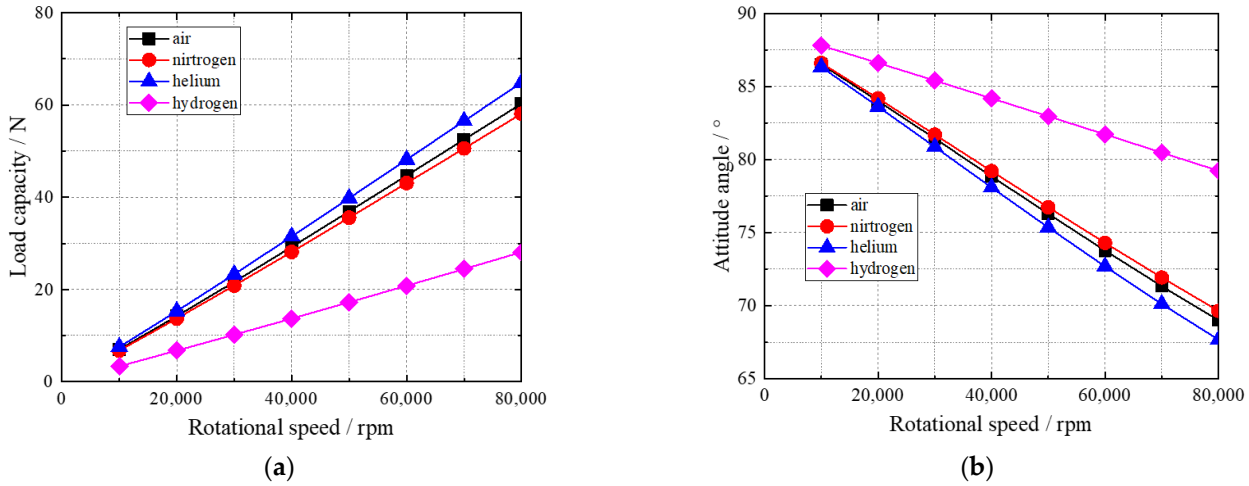

Figure 6. (**a**) Load capacities and (**b**) attitude angles with rotational speed using four different gases.

The friction torque with rotational speed obtained for the four different gases is shown in Figure 7. The values of bearing friction torque using air, nitrogen and helium are relatively close to one another. Throughout the whole speed range, the bearing friction torque using hydrogen is the lowest. In addition, the friction torque increases linearly with rotational speed.

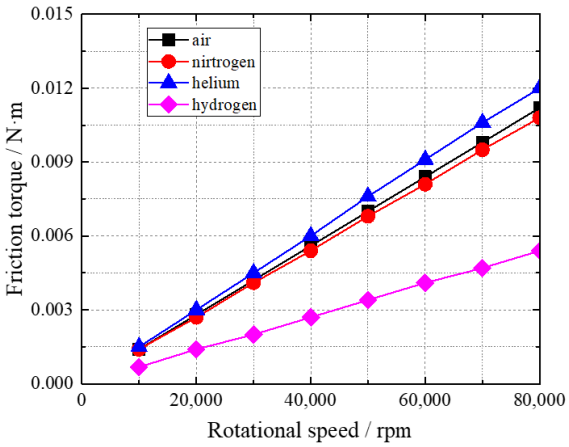

Figure 7. Bearing friction torque with rotational speed for the four different gases.

The critical masses of the bearings with rotational speed for the four different gases are shown in Figure 8. When the rotational speed is low, the critical mass is relatively high. The critical mass begins to decrease with increasing rotational speed. The critical mass of the helium-lubricated bearing is close to those of the air- and nitrogen-lubricated bearings, and all of them are higher than that of hydrogen-lubricated bearing. The critical masses of the bearings when using different gases can be ordered from high to low as: helium, air, nitrogen and hydrogen.

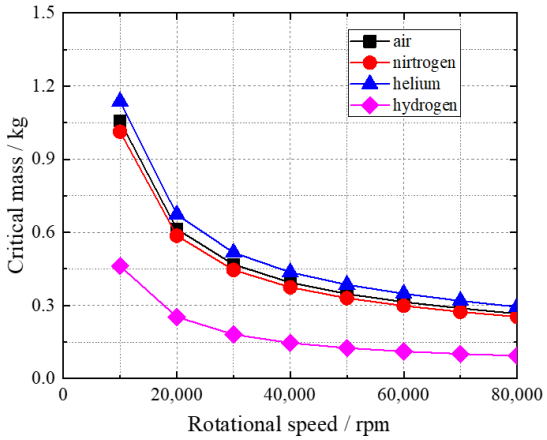

Figure 8. Critical masses of the bearings with rotational speed for the four different gases.

The influence of different gaseous lubricants on bearing performance is mainly due to differences in viscosity, which is consistent with the conclusions presented in the literature [22]. Therefore, when selecting lubricating gas, it is necessary to clarify the influence of gas viscosity under the designed conditions.

4. Influence Parameter Analysis

On the basis of the calculation results presented in the previous section, it can be seen that the performance of hydrogen gas bearings needs to be improved compared with other gas lubricated bearings. The effects of ambient pressure, gas film clearance and eccentricity ratio on the performance of hydrogen gas bearings are disclosed.

4.1. Ambient Pressure

The bearing load capacity and the attitude angle of hydrogen gas bearings with ambient pressure are shown in Figure 9. The load capacity increases slightly with increasing ambient pressure. Therefore, it is feasible to improve the bearing load capacity by increasing the ambient pressure. At the same time, the bearing attitude angle decreases gradually.

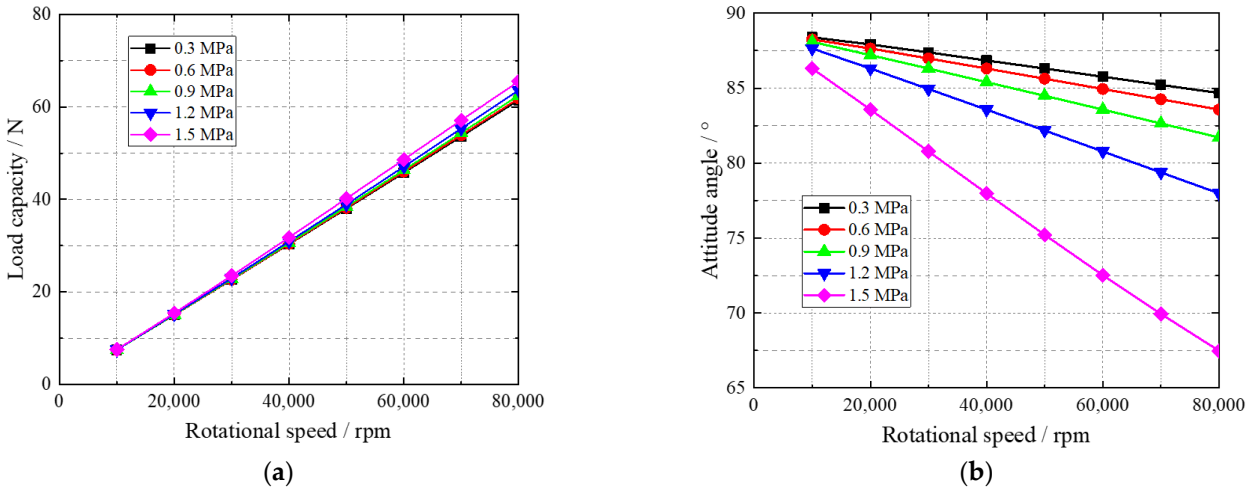

Figure 9. (**a**) Bearing load capacity and (**b**) attitude angle of hydrogen gas bearings with ambient pressure.

The friction torque of hydrogen gas bearings with ambient pressure is shown in Figure 10. The ambient pressure has a limited effect on the friction torque of the bearing. The friction loss is basically invariant with increasing ambient pressure.

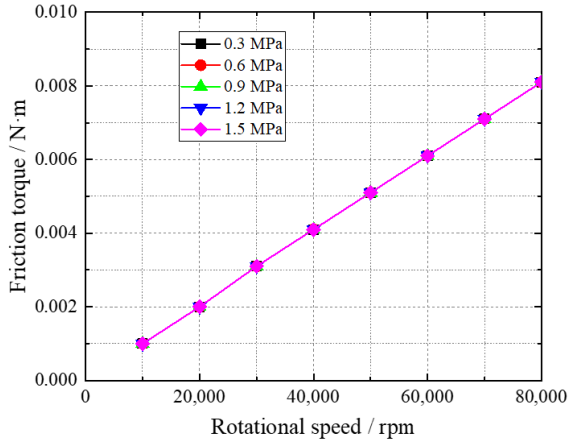

Figure 10. Friction torque of hydrogen gas bearings with ambient pressure.

The critical mass of hydrogen gas bearings with ambient pressure is shown in Figure 11. Higher ambient pressure leads to increasing critical mass. Overall, increasing the ambient pressure is also an effective method of enhancing the performance of hydrogen gas bearings.

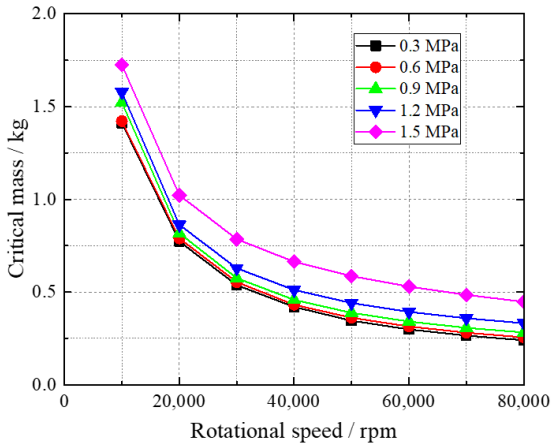

Figure 11. Critical mass of hydrogen gas bearings with ambient pressure.

4.2. Gas Film Clearance

Bearing film clearance has a great influence on the formation of wedge-shaped clearance, which directly affects bearing performance. The effects of different values of film clearance on bearing performance are calculated, while other parameters remain unchanged, as shown in Table 1. The load capacity and the attitude angle of hydrogen gas bearings with different film clearances are shown in Figure 12. The bearing load capacity increases with smaller values of gas film clearance. In addition, the difference in load capacity under different gas film clearance becomes greater at higher rotational speeds. Decreasing the gas film clearance is very effective for enhancing the bearing load capacity. Simultaneously, with decreasing gas film clearance, the bearing attitude angle exhibits a gradual decrease. The decrement of attitude angle increases with rotational speed.

The friction torque of hydrogen gas bearings with film clearance is shown in Figure 13. At larger values of gas film clearance, the friction torque of hydrogen gas bearings diminishes. Therefore, in the design stage, a compromise between load capacity and friction loss should be carefully considered.

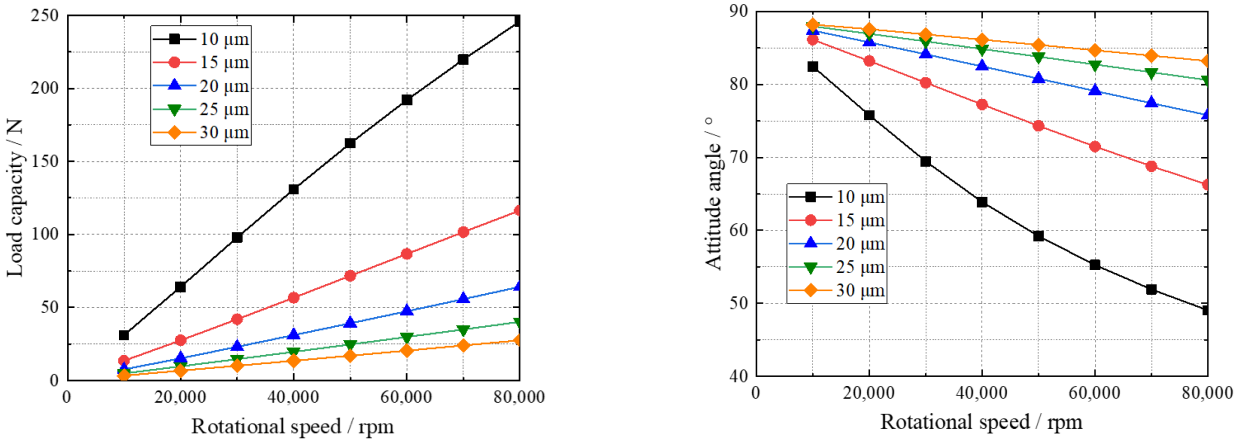

(**a**) (**b**)

Figure 12. (**a**) Bearing load capacity and (**b**) attitude angle of hydrogen gas bearings with gas film clearance.

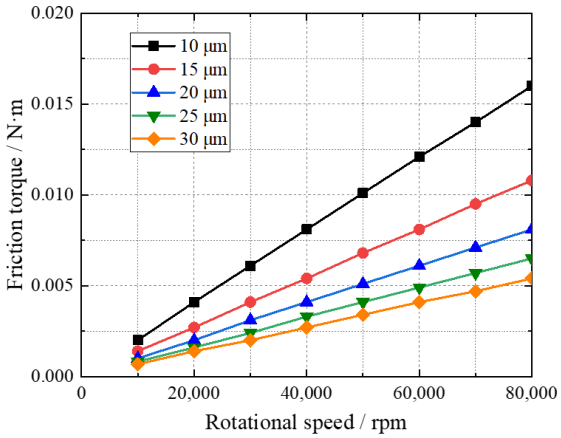

Figure 13. Friction torque of hydrogen gas bearings with gas film clearance.

The critical mass of hydrogen gas bearings with film clearance is shown in Figure 14. With decreasing film clearance, the critical mass of the hydrogen-lubricated bearings increases, improving the dynamic stability of the bearing.

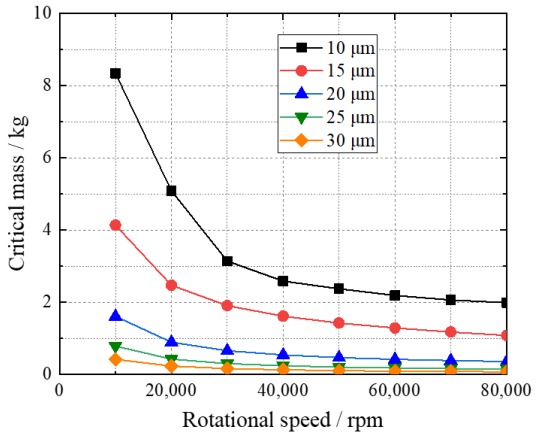

Figure 14. Critical mass of hydrogen gas bearings with gas film clearance.

4.3. Bearing Eccentricity Ratio

The eccentricity ratio of the bearing refers to the deviation between the rotor center and the bearing center to the gas film clearance, that is e/c_0. The difference in the size of the gas film clearance on both sides is caused by the eccentricity of the bearing, which has a great impact on the performance of the bearing. The influences of different eccentricity ratios on bearing performance are calculated while other parameters remain invariant, as shown in Table 1. The load capacity and attitude angle of hydrogen gas bearings with eccentricity ratio are shown in Figure 15. The bearing load capacity increases with the eccentricity ratio. In addition, the differences in load capacity under different eccentricity ratios increase with increasing rotational speed. Simultaneously, the attitude angle gradually decreases with increasing eccentricity ratio.

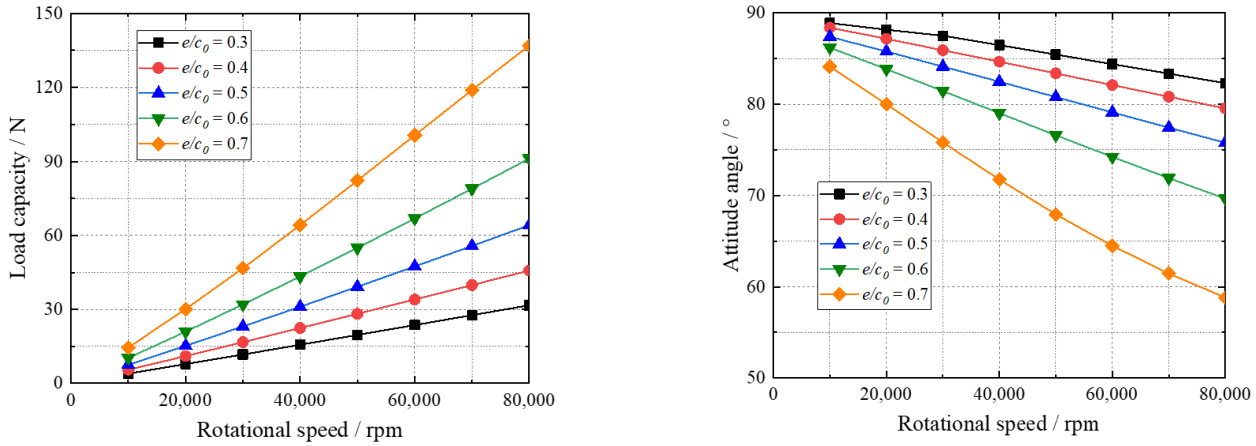

Figure 15. (**a**) Bearing load capacity and (**b**) attitude angle of hydrogen gas bearings with eccentricity ratio.

The friction torque of the hydrogen gas bearing with eccentricity ratio is shown in Figure 16. The friction torque of hydrogen gas bearings increases with increasing eccentricity ratio. In addition, the difference in friction torque under different eccentricity ratios increases with rotational speed.

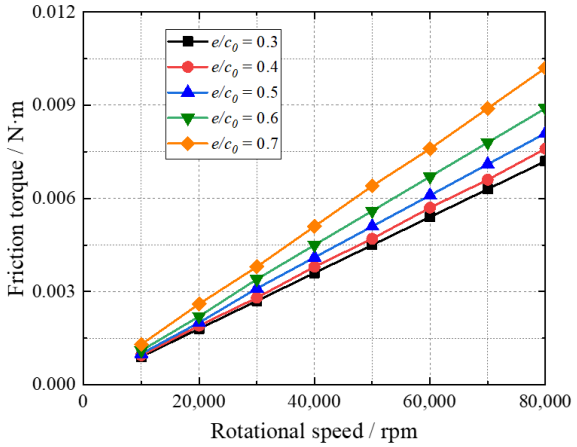

Figure 16. Friction torque of hydrogen gas bearings with eccentricity ratio.

The critical mass of hydrogen gas bearings with eccentricity ratio is shown in Figure 17. The critical mass of the hydrogen gas bearing increases with eccentricity ratio, and thus exhibits improved dynamic performance and stability.

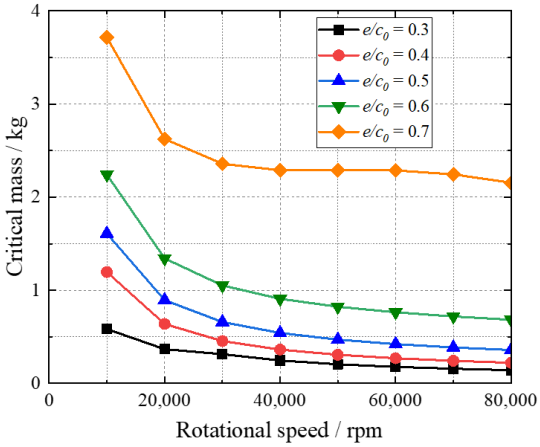

Figure 17. Critical mass of hydrogen gas bearings with eccentricity ratio.

4.4. Discussion and Analysis

To improve the load capacity and working stability of hydrogen gas bearings, increasing the ambient pressure, decreasing the gas film clearance, and increasing the bearing eccentricity ratio are quite effective. The main reasons for this are as follows:

- The augmentation of ambient pressure increases the average pressure in the gas film, which is beneficial to bearing performance.
- The reduction in gas film clearance promotes the formation of a wedge-shaped clearance, which improves the bearing load capacity and critical mass.
- The increment in the bearing eccentricity ratio also intensifies the formation of a wedge-shaped clearance, enhancing bearing load capacity and working stability.

5. Conclusions

In this paper, the performance of a gaseous hydrogen-lubricated herringbone grooved journal bearing was numerically calculated and compared with the performances of other commonly used gases. Bearing load capacity, friction torque and critical mass were used to quantify the performance of the bearing. Ambient pressure, gas film clearance, and bearing eccentricity ratio are factors that have an influence on bearing performance. On the basis of the above analysis, the following conclusions can be obtained:

(1) The physical properties of gas lubricants have a great influence on the bearing performance. The load capacity, friction torque, and critical mass of bearings of different gaseous lubricant decrease in the order of helium, air, nitrogen and hydrogen. In addition, the attitude angle of the bearings demonstrates a descending trend.

(2) Increasing ambient pressure can increase the bearing capacity and critical mass. Meanwhile, the attitude angle decreases, and the friction torque is not obviously affected. Therefore, increasing the ambient pressure can be regarded as an effective method for improving the bearing load.

(3) With decreasing gas film clearance and increasing bearing eccentricity ratio, the bearing load capacity, friction torque, and critical mass are enhanced, while the attitude angle decreases and operation stability is improved. Thus, lower gas film clearance and higher bearing eccentricity ratios can significantly boost the bearing performance.

Author Contributions: Data curation, M.Q.; formal analysis, M.Q., S.Y. and X.L.; resources, Q.Z.; supervision, T.L.; validation, M.Q.; writing—original draft, M.Q.; writing—review & editing, Y.H. and T.L. All authors have read and agreed to the published version of the manuscript.

Funding: This project was funded by the National Key R&D Program of China (2019YFB1504600).

Institutional Review Board Statement: This paper does not involve humans or animals.

Informed Consent Statement: This paper does not involve humans or animals.

Data Availability Statement: The study did not report any data.

Acknowledgments: Thanks for the support of the National Key R&D Program of China (2019YFB1504600).

Conflicts of Interest: The authors declare no conflict of interest.

References

1. Filippov, S.P.; Yaroslavtsev, A.B. Hydrogen energy: Development prospects and materials. *Russ. Chem. Rev.* **2021**, *90*, 627. [CrossRef]
2. Yamamoto, H.; Fujioka, H.; Okano, K. Cost analysis of stable electric and hydrogen energy supplies derived from 100% variable renewable resources systems. *Renew. Energy* **2021**, *178*, 1165–1173. [CrossRef]
3. Shikhar, U.; Hemmes, K.; Woudstra, T. Exploring the Possibility of Using Molten Carbonate Fuel Cell for the Flexible Coproduction of Hydrogen and Power. *Front. Energy Res.* **2021**, *9*, 394. [CrossRef]
4. Li, Y.; Kimura, S. Economic competitiveness and environmental implications of hydrogen energy and fuel cell electric vehicles in ASEAN countries: The current and future scenarios. *Energy Policy* **2021**, *148*, 111980. [CrossRef]
5. Tarhan, C.; Çil, M.A. A study on hydrogen, the clean energy of the future: Hydrogen storage methods. *J. Energy Storage* **2021**, *40*, 102676. [CrossRef]
6. Elberry, A.M.; Thakur, J.; Santasalo-Aarnio, A.; Larmi, M. Large-scale compressed hydrogen storage as part of renewable electricity storage systems. *Int. J. Hydrogen Energy* **2021**, *46*, 15671–15690. [CrossRef]
7. Aziz, M. Liquid Hydrogen: A Review on Liquefaction, Storage, Transportation, and Safety. *Energies* **2021**, *14*, 5917. [CrossRef]
8. Zhang, S.; Liu, G. Design and performance analysis of a hydrogen liquefaction process. *Clean Technol. Environ. Policy* **2022**, *24*, 51–65. [CrossRef]
9. Chang, H.M.; Kim, B.H.; Choi, B. Hydrogen liquefaction process with Brayton refrigeration cycle to utilize the cold energy of LNG. *Cryogenics* **2020**, *108*, 103093. [CrossRef]
10. Utlu, Z.; Karabuga, A. Conventional and enhanced exergy analysis of a hydrogen liquefaction system. *Int. J. Hydrogen Energy* **2020**, *46*, 2296–2305. [CrossRef]
11. Lai, T.; Guo, Y.; Zhao, Q.; Wang, Y.; Zhang, X.; Hou, Y. Numerical and Experimental Studies on Stability of Cryogenic Turbo-Expander with Protuberant Foil Gas Bearings. *Cryogenics* **2018**, *96*, 62–74. [CrossRef]
12. Faria, M.T.C. Some performance characteristics of high speed gas lubricated herringbone groove journal bearings. *JSME Int. J. Ser. C Mech. Syst. Mach. Elem. Manuf.* **2001**, *44*, 775–781. [CrossRef]
13. Gu, L.; Guenat, E.; Schiffmann, J. A Review of Grooved Dynamic Gas Bearings. *Appl. Mech. Rev.* **2020**, *72*, 010802. [CrossRef]
14. Hou, Y.; Lai, T.; Chen, S.; Ma, B.; Liu, J. Numerical analysis on the static performance of tilting pad–journal gas bearing in subsystems. *Tribol. Int.* **2013**, *61*, 70–79. [CrossRef]
15. Sim, K.; Lee, Y.B.; Song, J.W.; Kim, J.B.; Kim, T.H. Identification of the dynamic performance of a gas foil journal bearing operating at high temperatures. *J. Mech. Sci. Technol.* **2014**, *28*, 43–51. [CrossRef]
16. Li, S.S.; Chen, H.H.; Ding, H.B.; Zhang, G.Y.; Dong, M.L. Dynamic Performances of the Herringbone-Grooved Gas Bearing. In Proceedings of the IOP Conference Series: Materials Science and Engineering 2018, Dalian, China, 1–3 July 2018; Volume 408. [CrossRef]
17. Li, J.; Yang, S.Q.; Li, X.M.; Wu, J.H.; Li, Q. CFD research on hydrodynamic gas bearings with different styles of grooves. In Proceedings of the IOP Conference Series: Materials Science and Engineering 2017, Madison, WI, USA, 9–13 July 2017; Volume 278. [CrossRef]
18. Li, Y.; Liu, J.; Li, L.; Yang, D. Effect of environmental pressure on dynamic characteristics of aerodynamic gas bearing of boost turbo expander. In Proceedings of the IOP Conference Series: Materials Science and Engineering 2018, Nanjing, China, 23–26 May 2018; Volume 382. [CrossRef]
19. Zagarola, M.V.; Cragin, K.J.; McCormick, J.A. Operation of gas bearings at cryogenic temperatures. *Cryogenics* **2020**, *105*, 103001. [CrossRef]
20. Davydov, A.B.; Sherstyuk, A.N. Features distinguishing hydrogen turboexpanders from air turboexpanders. *Chem. Pet. Eng.* **1996**, *32*, 453–456. [CrossRef]
21. Davydenkov, I.A.; Davydov, A.B.; Perestoronin, G.A. Hydrogen and nitrogen turboexpanders with high gas expansion ratios. *Cryogenics* **1992**, *32*, 84–86. [CrossRef]
22. Guo, Y.; Lai, T.; Ren, X.; Zhao, Q.; Hou, Y. Effect of lubrication medium on gas bearing performance. *Lubr. Eng.* **2021**, *46*, 1–5. [CrossRef]
23. Yan, H.; Ke, C.; Peng, N.; Li, K.; Zhang, X.; Xiong, L.; Dong, B.; Li, J.; Liu, L. Performance prediction of externally pressurized gas bearings for high-speed turbo-expander involving hydrogen, helium and air working fluids. *Int. J. Hydrogen Energy* **2021**, *46*, 33453–33467. [CrossRef]
24. Reynolds, O. On the theory of lubrication and its application to Mr. beauchamp tower's experiments, including an experimental determination of the viscosity of olive oil. *Phil. Trans. Roy. Soc. A* **1885**, *1*, 157.

25. Constantinescu, V.N. Basic Relationships in Turbulent Lubrication and Their Extension to Include Thermal Effects. *J. Lubr. Technol.* **1973**, *95*, 147–154. [CrossRef]
26. Lund, J.W. Calculation of stiffness and damping properties of gas bearings. *J. Lubr. Technol.* **1968**, *90*, 793. [CrossRef]
27. Klit, P.; Lund, J.W. Calculation of the dynamic coefficients of a journal bearing, using a variational approach. *J. Tribol.* **1986**, *108*, 421–425. [CrossRef]
28. Ho, M.T.; Datta, A.; Bhattacharyya, S.P. An elementary derivation of the routh-hurwitz criterion. *IEEE Trans. Autom. Control* **1998**, *43*, 405–409.
29. Bonneau, D.; Absi, J. Analysis of aerodynamic journal bearings with small number of herringbone grooves by finite element method. *J. Tribol.* **1994**, *116*, 698–704. [CrossRef]